Reactive Power Compensation and Negative-Sequence Current Suppression System for Electrical Railways With YNvd-Connected Balance Transformer—Part I: Theoretical Analysis

Zhiwen Zhang, Bin Xie, Sijia Hu, *Member, IEEE*, Yong Li, *Senior Member, IEEE*, Longfu Luo, *Member, IEEE*, Christian Rehtanz, *Senior Member, IEEE*, and Olav Krause, *Member, IEEE*

***Abstract*—This paper presents a new system for reactive power compensation and suppression of negative-sequence current for power quality improvement in electrical railways and the feeding three-phase utility grid, based on YNvd-connected balance transformer. Different from the conventional railway static power conditioner based compensation systems, this system integrates multiplex back-to-back converters (MBTBC) into phase-β side flexible taps through a cascade connection instead of into phase-β side feeder via a coupling transformer, thus the installation space and initial costs are reduced significantly. In addition, a new power distribution strategy with simple implementation is adopted in this paper, by which the compensation capacity of MBTBC can be decreased by 25%, compared with the commonly used full compensation scheme. As the first part of this topic, this paper focuses on the theoretical analysis, including the system topology, basic and partial compensation principles and its implementation method. While, the controller design on converter-level, stability analysis, and simulation and experimental verification are the main tasks of the second part of this topic.**

***Index Terms*—Balance transformer, electrical railway, multiplex back-to-back converters (MBTBC), partial compensation.**

I. Introduction

POWER quality problems, such as high current distortion, low power factor, and severe three-phase current and voltage unbalance, exist widely in electrical railway power system (ERPS) [1], which are particularly prominent in the running sections of phase-controlled locomotives [2]. Though the pulse width modulation (PWM) based new generation trains are launched in Chinese railway system, the power quality in ERPS is still far from satisfactory because of the high penetration rate of the commissioned traditional locomotives [3], [4]. Besides, the large power consumption of the new generation trains aggravates the unbalance performance of ERPS [5], though the low-order harmonics and reactive power can be eliminated by its PWM front-end rectifiers [6].

Passive *LC* filters, with the merits of high efficiency and low costs, are often adopted for harmonic currents filtering and reactive power compensating in the investment restricted construction projects of ERPS [7], [8]. However, the fixed compensation scheme may not fully satisfy the reactive power demand of the various railway loads [9]. Besides, the resonance risk of the *LC*-branches also forces the engineers to do more efforts in the designing process [10]. Balance transformers, which are widely used in ERPS, are inherently able to suppress negative-sequence current (NSC) better than other traction transformers (e.g., Vv connection transformer) [11]. But it cannot compensate reactive power and harmonics, and the NSC suppression ability is also affected by the load conditions in some extent [12].

Combining power electronic devices and passive elements together properly, many active and hybrid compensation methods are introduced and studied [13]–[33]. Static voltage-ampere (VA) reactive (Var) compensators (SVCs), usually associated with filter branches, can be applied to compensate reactive power, harmonics, NSC, and stabilize feeder voltage in ERPS [13]–[15]. But the low integration level, relatively slow response speed, and resonance risk fade its comprehensive performance. By the use of all-controlling power electronic devices and advanced control algorithms, static synchronous compensators (STATCOMs) can avoid the drawbacks of SVC [16]–[19]. Three-phase STATCOM can relieve reactive power and NSC problems [20], [21], and it can also be installed at the primary side of ERPS for power quality improvement [22]. But a high-voltage three-phase step-down transformer is required. Single-phase STATCOMs can be applied to the feeders of ERPS with relatively low isolation requirement, the NSC problem, however,

Manuscript received August 18, 2016; revised November 7, 2016 and January 4, 2017; accepted February 7, 2017. Date of publication February 16, 2017; date of current version October 6, 2017. This work was supported in part by the National Nature Science Foundation of China under Grant 51477046 and Grant 51377001 and in part by the International Science and Technology Cooperation Program of China under Grant 2015DFR70850. Recommended for publication by Associate Editor Z. Li. *(Corresponding author: Sijia Hu.)*

Z. Zhang, B. Xie, S. Hu, Y. Li, and L. Luo are with the College of Electrical and Information Engineering, Hunan University, Changsha 410082, China (e-mail: hdzzw@126.com; xiebin_1215@163.com; huda_hsj@163.com; yongli@hnu.edu.cn; llf@hnu.edu.cn).

C. Rehtanz is with the Institute of Energy Systems, Energy Efficiency and Energy Economics, TU Dortmund University, Dortmund 44227, Germany (e-mail: christian.rehtanz@tu-dortmund.de).

O. Krause is with the School of Information Technology and Electrical Engineering, the University of Queensland, Brisbane QLD 4072, Australia (e-mail: o.krause@uq.edu.au).

Color versions of one or more of the figures in this paper are available online at http://ieeexplore.ieee.org.

Digital Object Identifier 10.1109/TPEL.2017.2670082

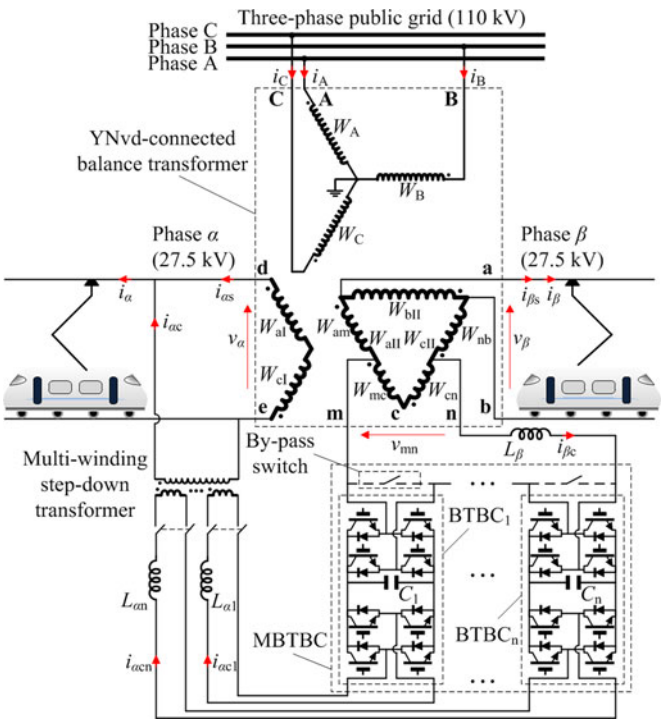

Fig. 1. Topology of the proposed system.

cannot be fully solved because it has no path to balance the active power of the two-phase loads [23], [24]. A three-phase converter, as a main component of APQC (see [25]), can be interfaced to ERPS's feeders via one Scott transformer with satisfactory power quality management performance. The complex high-power Scott transformer, however, will certainly increase the costs of the whole system. By rebalancing the active power of two-phase loads and compensating reactive power or harmonics of each feeder independently, railway static power conditioner (RPC) [26], [27], which evolves from the single-phase converter, can deal with almost all the power quality problems in ERPS. To make the back-to-back converter unit galvanic isolation and get proper interface voltages, two single-phase multiwinding isolation transformers, which are giant and expensive in practical applications, are indispensable in the RPC-based compensation systems. Hybrid compensation methods, which cut down the ratings of active facilities effectively by sharing the burden of reactive compensating and harmonic filtering with some carefully designed *LC*-branches, draw much attention recently [28]–[31]. And by pursuing compromising instead of full compensation goals (i.e., unit primary power factor, no NSC) [32], partial compensation methods can also be applied in electrical railway compensation systems to reduce the power ratings of the active facilities [32], [33]. However, those achievements are just obtained at the not so popular cophase ERPS.

To explore a compensation system with less area occupation, lower VA-capacity, and simpler controller implementation, a comprehensive study of a new power quality improvement system for ERPS, which is based on YNvd-connected balance transformer, is presented in this paper (see Fig. 1). By taking the advantages of the asymmetric secondary windings ("v" and "Δ" windings) and flexible taps (m and n, which can be adjusted in the designing stage) of the main transformer, only one step-down isolation transformer is required, and so the system's integration level is greatly improved. In addition, by using the perpendicular characteristic of the two-phase feeder voltages, a new power distribution strategy, which involves no complex optimization process, is explored in detail for the usually adopted two-phase ERPS. Based on this new strategy, the VA capacity of the converter can be decreased by 25% in comparison to the commonly used full compensation strategy, so the costs and power losses of the active facilities can be decreased. By the way, considering a full discussion on this topic in a length-limited paper is challengeable, so the controller design on converter level, stability problems, and comprehensive simulation and experimental verification of the proposed system are given in Part II, as a sister paper of this part on theoretical analysis. The organization of this part is as follows. The system topology is discussed in Section II. Section III presents the basic compensation principle. The new partial compensation strategy and the related implementation method are clearly analyzed in Section IV. Section V is the conclusion of this part.

II. Topology

It can be seen in Fig. 1 that a YNvd-connected balance transformer can not only feed locomotives on phase α and β via terminals d-e and a-b, but also have the potential to supply power to three-phase loads via taps m, n, and c [11]. Compared with the commonly applied impedance-matching transformer and Scott transformer in ERPS, YNvd-connected balance transformer is relatively simple and easy in the designing stage, though balance transformers are often more complex than Vv connection transformer. In addition, the naturally asymmetric "v" and "Δ" windings give the system a great potential to be integrated with some power electronics systems. In the proposed system, multiplex back-to-back converters (MBTBC), which is constructed with units $\mathrm{BTBC}_1-\mathrm{BTBC}_n$, are responsible for reactive power compensation and active power transmission. Since the turns' number of windings mc and cn can be specifically adjusted, together with the cascade structure adopted by the phase-β side terminals of MBTBC, no coupling transformer is required on this side. Considering the other terminals of MBTBC are parallel connected with the secondary windings of a multiwinding step-down transformer, the output voltages of both sides of MBTBC can be properly matched. Besides, because the active power among different units can be exchanged due to the adoption of the multiwinding step-down transformer, so the self-balance capability of dc link among different units (see the secondary part of this paper) is obtained in this proposed system.

As a conclusion, the advantages of the proposed system topology are listed below:

1) Since the turns' ratio of taps m and n can be adjusted in the designing process of YNvd-connected balance transformer, v_{mn} can be set directly to the level of MBTBC, and thus the system integration can be greatly enhanced.
2) The isolation together with the voltage match issues of MBTBC are solved by the multiwinding step-down

transformer (note: short circuits will occur if no isolation is provided).

3) This system features modularity, and relatively high system reliability can be obtained further if the by-pass switches (see Fig. 1) are installed.

III. Basic Compensation Principle

Referring to Fig. 1, we define

$$\begin{cases} W_{\mathrm{A}} = W_{\mathrm{B}} = W_{\mathrm{C}} = W_1 \\ W_{\mathrm{aII}} = W_{\mathrm{bII}} = W_{\mathrm{cII}} = W_2 \\ W_{\mathrm{aI}} = W_{\mathrm{cI}} = W_3 \\ W_{\mathrm{mc}} = xW_{\mathrm{aII}}, W_{\mathrm{cn}} = xW_{\mathrm{cII}} \\ \mathbf{Z}_{\mathrm{aII}} = \mathbf{Z}_{\mathrm{bII}} = \mathbf{Z}_{\mathrm{cII}} = \mathbf{Z}_2 \\ \mathbf{Z}_{\mathrm{aI}} = \mathbf{Z}_{\mathrm{cI}} = \mathbf{Z}_1 \\ \mathbf{Z}_{\mathrm{mc}} = \lambda \mathbf{Z}_{\mathrm{aII}}, \mathbf{Z}_{\mathrm{cn}} = \lambda \mathbf{Z}_{\mathrm{cII}} \end{cases} \tag{1}$$

where $W_2/W_3 = 1.732$, and $\mathbf{Z}_{\mathrm{aII}}$, $\mathbf{Z}_{\mathrm{bII}}$, $\mathbf{Z}_{\mathrm{cII}}$, $\mathbf{Z}_{\mathrm{aI}}$, $\mathbf{Z}_{\mathrm{cI}}$, $\mathbf{Z}_{\mathrm{mc}}$, and $\mathbf{Z}_{\mathrm{cn}}$ represent the equivalent leakage impedances of the corresponding windings. To satisfy the balance condition, the turns ratio x and the impedance ratio λ between winding mc (cn) and ac (cb) should be equal [34], which is explained in Appendix A.

Based on the definitions in (1), the relationships of the primary and secondary currents can be discussed according to the equivalent circuit, as shown in Fig. 2(a). First, the superposition principle and Kirchhoff's law regulate the currents as

$$\begin{cases} \mathbf{I}_{\mathrm{a1}} = -\mathbf{I}_{\mathrm{c1}} = \mathbf{I}_{\alpha \mathrm{c}} - \mathbf{I}_{\alpha} \\ \mathbf{I}_{\mathrm{a2}} = \mathbf{I}_{\mathrm{c2}} = -1/3\mathbf{I}_{\beta} - 2x/3\mathbf{I}_{\beta \mathrm{c}} \\ \mathbf{I}_{\mathrm{a3}} = \mathbf{I}_{\mathrm{c3}} = -1/3\mathbf{I}_{\beta} + (3-2x)/3\mathbf{I}_{\beta \mathrm{c}} \\ \mathbf{I}_{\mathrm{b}} = 2/3\mathbf{I}_{\beta} - 2x/3\mathbf{I}_{\beta \mathrm{c}}. \end{cases} \tag{2}$$

Ignoring the magnetizing currents, the ampere-turns balance equations of the traction transformer can be listed as

$$\begin{cases} \text{Phase A} : \mathbf{I}_{\mathrm{A}} W_1 + \mathbf{I}_{\mathrm{a1}} W_3 + (1-x)\mathbf{I}_{\mathrm{a2}} W_2 + x\mathbf{I}_{\mathrm{a3}} \mathrm{W}_2 = \mathbf{0} \\ \text{Phase B} : \mathbf{I}_{\mathrm{B}} W_1 + \mathbf{I}_{\mathrm{b}} W_2 = \mathbf{0} \\ \text{Phase C} : \mathbf{I}_{\mathrm{C}} W_1 + \mathbf{I}_{\mathrm{c1}} W_3 + (1-x)\mathbf{I}_{\mathrm{c2}} W_2 + x\mathbf{I}_{\mathrm{c3}} W_2 = \mathbf{0}. \end{cases} \tag{3}$$

Combining (2) and (3), the primary currents $\mathbf{I}_{\mathrm{A}}$, $\mathbf{I}_{\mathrm{B}}$, $\mathbf{I}_{\mathrm{C}}$, and the secondary currents $\mathbf{I}_{\alpha}$, $\mathbf{I}_{\beta}$ and $\mathbf{I}_{\alpha \mathrm{c}}$, $\mathbf{I}_{\beta \mathrm{c}}$ satisfy

$$\begin{aligned} \begin{bmatrix} \mathbf{I}_{\mathrm{A}} \\ \mathbf{I}_{\mathrm{B}} \\ \mathbf{I}_{\mathrm{C}} \end{bmatrix} &= \frac{1}{3K} \begin{bmatrix} \sqrt{3} & 1 \\ 0 & -2 \\ -\sqrt{3} & 1 \end{bmatrix} \begin{bmatrix} \mathbf{I}_{\alpha} \\ \mathbf{I}_{\beta} \end{bmatrix} + \frac{1}{3K} \begin{bmatrix} -\sqrt{3} & x \\ 0 & -2x \\ \sqrt{3} & x \end{bmatrix} \begin{bmatrix} \mathbf{I}_{\alpha \mathrm{c}} \\ \mathbf{I}_{\beta \mathrm{c}} \end{bmatrix} \\ &= \mathbf{S}_1 \begin{bmatrix} \mathbf{I}_{\alpha} \\ \mathbf{I}_{\beta} \end{bmatrix} + \mathbf{S}_2 \begin{bmatrix} \mathbf{I}_{\alpha \mathrm{c}} \\ \mathbf{I}_{\beta \mathrm{c}} \end{bmatrix} \end{aligned} \tag{4}$$

where the transformer ratio $K = W_1/W_2 = 2.309$. The current transformation matrices, which are determined by the electromagnetic characteristics of YNvd-connected balance transformer, are presented by $\mathbf{S}_1$ and $\mathbf{S}_2$.

Canceling the undesired parts in $\mathbf{I}_{\alpha}$ and $\mathbf{I}_{\beta}$ by injecting the compensation currents $\mathbf{I}_{\alpha \mathrm{c}}$ and $\mathbf{I}_{\beta \mathrm{c}}$, a satisfactory performance can be obtained. To make a quantitative analysis, referring to

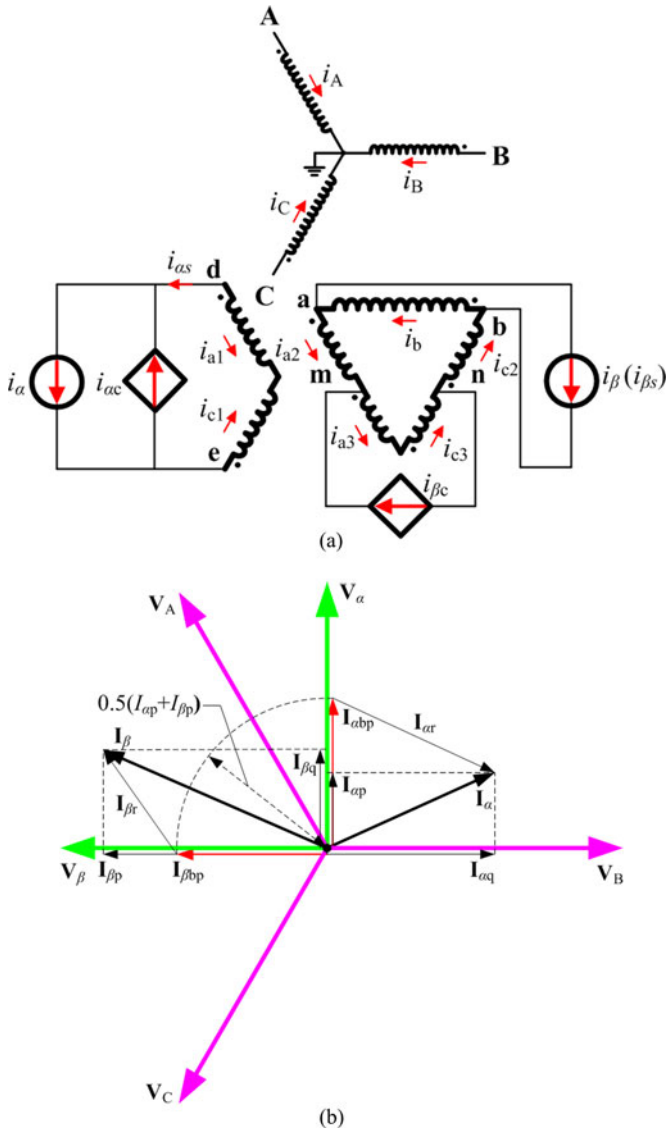

Fig. 2. Compensation principle. (a) Equivalent circuit. (b) Phasor relationships of full compensation mode.

Fig. 2(a), a reference frame of voltage is defined as

$$\begin{cases} \mathbf{V}_{\mathrm{A}} = V_{\mathrm{A}} \angle 120^\circ, \mathbf{V}_{\mathrm{B}} = V_{\mathrm{B}} \angle 0^\circ, \mathbf{V}_{\mathrm{C}} = V_{\mathrm{C}} \angle -120^\circ \\ \mathbf{V}_{\alpha} = V_{\alpha} \angle 90^\circ, \mathbf{V}_{\beta} = V_{\beta} \angle 180^\circ. \end{cases} \tag{5}$$

Fig. 2(b) shows the phasor relationships of full compensation mode. From Fig. 2(b), we divide $\mathbf{I}_{\alpha}$ and $\mathbf{I}_{\beta}$ into balanced active parts $\mathbf{I}_{\alpha \mathrm{bp}}$, $\mathbf{I}_{\beta \mathrm{bp}}$ [$\mathbf{I}_{\alpha \mathrm{bp}} = I_{\alpha \mathrm{bp}} \angle 90^\circ$, $\mathbf{I}_{\beta \mathrm{bp}} = I_{\beta \mathrm{bp}} \angle 180^\circ$, and $I_{\alpha \mathrm{bp}} = I_{\beta \mathrm{bp}} = 0.5(I_{\alpha \mathrm{p}} + I_{\beta \mathrm{p}})$] and undesired parts $\mathbf{I}_{\alpha \mathrm{r}}$, $\mathbf{I}_{\beta \mathrm{r}}$, i.e.,

$$\begin{bmatrix} \mathbf{I}_{\alpha} \\ \mathbf{I}_{\beta} \end{bmatrix} = \begin{bmatrix} \mathbf{I}_{\alpha \mathrm{bp}} \\ \mathbf{I}_{\beta \mathrm{bp}} \end{bmatrix} + \begin{bmatrix} \mathbf{I}_{\alpha \mathrm{r}} \\ \mathbf{I}_{\beta \mathrm{r}} \end{bmatrix}. \tag{6}$$

Inserting (6) into (4), $\mathbf{I}_{\mathrm{A}}$, $\mathbf{I}_{\mathrm{B}}$, $\mathbf{I}_{\mathrm{C}}$ can be represented by

$$\begin{bmatrix} \mathbf{I}_{\mathrm{A}} \\ \mathbf{I}_{\mathrm{B}} \\ \mathbf{I}_{\mathrm{C}} \end{bmatrix} = \mathbf{S}_1 \begin{bmatrix} \mathbf{I}_{\alpha \mathrm{bp}} \\ \mathbf{I}_{\beta \mathrm{bp}} \end{bmatrix} + \mathbf{S}_1 \begin{bmatrix} \mathbf{I}_{\alpha \mathrm{r}} \\ \mathbf{I}_{\beta \mathrm{r}} \end{bmatrix} + \mathbf{S}_2 \begin{bmatrix} \mathbf{I}_{\alpha \mathrm{c}} \\ \mathbf{I}_{\beta \mathrm{c}} \end{bmatrix}. \tag{7}$$

In order to eliminate $\mathbf{I}_{\alpha\mathrm{r}}$ and $\mathbf{I}_{\beta\mathrm{r}}$, the last two terms in (7) should satisfy the following equation:

$$\mathbf{S}_1 \begin{bmatrix} \mathbf{I}_{\alpha\mathrm{r}} \\ \mathbf{I}_{\beta\mathrm{r}} \end{bmatrix} + \mathbf{S}_2 \begin{bmatrix} \mathbf{I}_{\alpha\mathrm{c}} \\ \mathbf{I}_{\beta\mathrm{c}} \end{bmatrix} = \mathbf{0}. \tag{8}$$

Inserting $\mathbf{I}_{\alpha\mathrm{bp}}$, $\mathbf{I}_{\beta\mathrm{bp}}$ and (8) into (7), the primary currents under the reference frame can be derived as follows:

$$\begin{aligned} \begin{bmatrix} \mathbf{I}_{\mathrm{A}} \\ \mathbf{I}_{\mathrm{B}} \\ \mathbf{I}_{\mathrm{C}} \end{bmatrix} &= \mathbf{S}_1 \begin{bmatrix} \mathbf{I}_{\alpha\mathrm{bp}} \\ \mathbf{I}_{\beta\mathrm{bp}} \end{bmatrix} = \underbrace{\frac{2}{3K}}_{\sigma} \begin{bmatrix} \sqrt{3}/2 & 1/2 \\ 0 & -1 \\ -\sqrt{3}/2 & 1/2 \end{bmatrix} \begin{bmatrix} \mathbf{I}_{\alpha\mathrm{bp}} \\ \mathbf{I}_{\beta\mathrm{bp}} \end{bmatrix} \\ &= \sigma I_{\alpha\mathrm{bp}} \begin{bmatrix} 1\angle 120^\circ \\ 1\angle 0^\circ \\ 1\angle -120^\circ \end{bmatrix} \end{aligned} \tag{9}$$

where $\sigma = 0.2887$. It can be observed from (5) and (9) that $\mathbf{I}_{\mathrm{A}}$, $\mathbf{I}_{\mathrm{B}}$, $\mathbf{I}_{\mathrm{C}}$ are balanced with no-phase displacement separately to their voltages. The full compensation is obtained.

From (8), $\mathbf{I}_{\alpha\mathrm{c}}$ and $\mathbf{I}_{\beta\mathrm{c}}$ can be calculated as follows:

$$\begin{bmatrix} \mathbf{I}_{\alpha\mathrm{c}} \\ \mathbf{I}_{\beta\mathrm{c}} \end{bmatrix} = \begin{bmatrix} 1 & 0 \\ 0 & 1/x \end{bmatrix} \begin{bmatrix} \mathbf{I}_{\alpha\mathrm{r}} \\ \mathbf{I}_{\beta\mathrm{r}} \end{bmatrix} = \mathbf{S} \begin{bmatrix} \mathbf{I}_{\alpha\mathrm{r}} \\ \mathbf{I}_{\beta\mathrm{r}} \end{bmatrix} \tag{10}$$

In fact, by replacing $\mathbf{I}_{\alpha\mathrm{r}}$ and $\mathbf{I}_{\beta\mathrm{r}}$ in (10) with any kinds of other undesired components in $\mathbf{I}_\alpha$ and $\mathbf{I}_\beta$ (e.g., partial of $\mathbf{I}_{\alpha\mathrm{r}}$ and $\mathbf{I}_{\beta\mathrm{r}}$), a flexible compensation scheme can be obtained, which is the main discussion point of Section IV.

IV. New Partial Compensation Strategy

A. Compensation Goals

For reactive power reduction and NSC mitigation, the best performance is unity power factor and no NSC in the primary side. But the results are not always necessary in real applications for the consideration of the investments and the related power quality standards. Hence, it is better to develop a partial power distribution method. First, we define the compensation goals as

$$\begin{cases} \mathrm{PF_f} = \sum_{\mathrm{k=A,B,C}} P_{\mathrm{k}} \Big/ \sum_{\mathrm{k=A,B,C}} S_{\mathrm{k}} = \sum_{\mathrm{k=A,B,C}} I_{\mathrm{kp}} \Big/ \\ \qquad \sum_{\mathrm{k=A,B,C}} I_{\mathrm{k}} \geq 0.9 \\ \mathrm{I_{unb}} = I_- / I_+ \times 100\% \leq 10\% \end{cases} \tag{11}$$

where $\mathrm{PF_f}$ and $\mathrm{I_{unb}}$ mean the fundamental power factor and NSC unbalance ratio, separately; P_{k} and S_{k} are the fundamental active power and apparent power of the primary three phases, respectively; I_{k} are the amplitude of the fundamental primary three-phase currents; I_{kp} represent the amplitude of the active power components of I_{k}; I_- and I_+ denote the amplitude of the fundamental NSC and positive-sequence current (PSC), separately.

Although the negative-sequence voltage unbalance ratio ($\mathrm{U_{unb}} = V_-/V_+$) is adopted in Chinese unbalance standard (i.e., $\mathrm{U_{unb}} \leq 2\%$ [35]), $\mathrm{I_{unb}} \leq 10\%$ is adopted as a criterion in this paper. Generally speaking, due to the usually small three-phase-grid source impedance, $\mathrm{I_{unb}} \leq 10\%$ is stricter than $\mathrm{U_{unb}} \leq 2\%$ and PF_f can also be evaluated, as shown in (11).

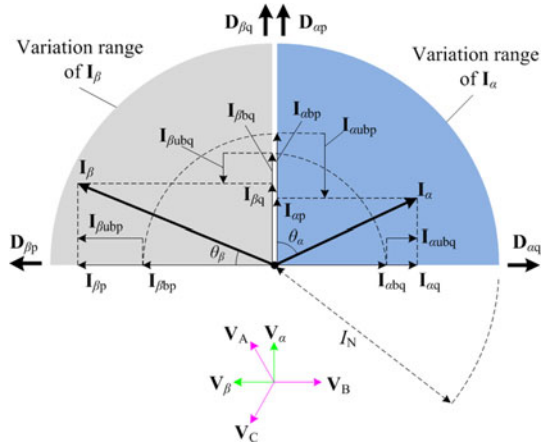

Fig. 3. Phasor relationships of general locomotive loads.

B. Derivation of $\mathrm{PF_f}$ and $\mathrm{I_{unb}}$ on the Basis of Load Currents' Components

Based on the phasor diagram of general load currents shown in Fig. 3 (I_N is the nominal value of load currents), we can divide $\mathbf{I}_\alpha$ (or $\mathbf{I}_\beta$) into active and reactive components $\mathbf{I}_{\alpha\mathrm{p}}$ (or $\mathbf{I}_{\beta\mathrm{p}}$) and $\mathbf{I}_{\alpha\mathrm{q}}$ (or $\mathbf{I}_{\beta\mathrm{q}}$). And $\mathbf{I}_{\alpha\mathrm{p}}$ (or $\mathbf{I}_{\beta\mathrm{p}}$) and $\mathbf{I}_{\alpha\mathrm{q}}$ (or $\mathbf{I}_{\beta\mathrm{q}}$) can be further separated as balanced and unbalanced parts $\mathbf{I}_{\alpha\mathrm{bp}}$, $\mathbf{I}_{\alpha\mathrm{bq}}$ (or $\mathbf{I}_{\beta\mathrm{bp}}$, $\mathbf{I}_{\beta\mathrm{bq}}$) and $\mathbf{I}_{\alpha\mathrm{ubp}}$, $\mathbf{I}_{\alpha\mathrm{ubq}}$ (or $\mathbf{I}_{\beta\mathrm{ubp}}$, $\mathbf{I}_{\beta\mathrm{ubq}}$), respectively. Therefore, $\mathbf{I}_\alpha$ and $\mathbf{I}_\beta$ can be rewritten as

$$\begin{cases} \mathbf{I}_\alpha = \underbrace{\underbrace{\overbrace{0.5(I_{\alpha\mathrm{p}} + I_{\beta\mathrm{p}})}^{I_{\alpha\mathrm{bp}}}\mathbf{D}_{\alpha\mathrm{p}}}_{\mathbf{I}_{\alpha\mathrm{bp}}} + \underbrace{\overbrace{0.5(I_{\alpha\mathrm{p}} - I_{\beta\mathrm{p}})}^{I_{\alpha\mathrm{ubp}}}\mathbf{D}_{\alpha\mathrm{p}}}_{\mathbf{I}_{\alpha\mathrm{ubp}}}}_{\mathbf{I}_{\alpha\mathrm{p}}} \\ \qquad + \underbrace{\underbrace{\overbrace{0.5(I_{\alpha\mathrm{q}} + I_{\beta\mathrm{q}})}^{I_{\alpha\mathrm{bq}}}\mathbf{D}_{\alpha\mathrm{q}}}_{\mathbf{I}_{\alpha\mathrm{bq}}} + \underbrace{\overbrace{0.5(I_{\alpha\mathrm{q}} - I_{\beta\mathrm{q}})}^{I_{\alpha\mathrm{ubq}}}\mathbf{D}_{\alpha\mathrm{q}}}_{\mathbf{I}_{\alpha\mathrm{ubq}}}}_{\mathbf{I}_{\alpha\mathrm{q}}} \\ \mathbf{I}_\beta = \underbrace{\underbrace{\overbrace{0.5(I_{\alpha\mathrm{p}} + I_{\beta\mathrm{p}})}^{I_{\beta\mathrm{bp}}}\mathbf{D}_{\beta\mathrm{p}}}_{\mathbf{I}_{\beta\mathrm{bp}}} + \underbrace{\overbrace{0.5(I_{\beta\mathrm{p}} - I_{\alpha\mathrm{p}})}^{I_{\beta\mathrm{ubp}}}\mathbf{D}_{\beta\mathrm{p}}}_{\mathbf{I}_{\beta\mathrm{ubp}}}}_{\mathbf{I}_{\beta\mathrm{p}}} \\ \qquad + \underbrace{\underbrace{\overbrace{0.5(I_{\alpha\mathrm{q}} + I_{\beta\mathrm{q}})}^{I_{\beta bq}}\mathbf{D}_{\beta\mathrm{q}}}_{\mathbf{I}_{\beta\mathrm{bq}}} + \underbrace{\overbrace{0.5(I_{\beta\mathrm{q}} - I_{\alpha\mathrm{q}})}^{I_{\beta\mathrm{ubq}}}\mathbf{D}_{\beta\mathrm{q}}}_{\mathbf{I}_{\beta\mathrm{ubq}}}}_{\mathbf{I}_{\beta\mathrm{q}}} \end{cases} \tag{12}$$

where $\mathbf{D}_{\alpha\mathrm{p}} = \mathbf{D}_{\beta\mathrm{q}} = 1\angle 90^\circ$, $\mathbf{D}_{\alpha\mathrm{q}} = 1\angle 0^\circ$, and $\mathbf{D}_{\beta\mathrm{p}} = 1\angle 180^\circ$.

Based on the above divisions, $\mathbf{I}_\alpha$ (or $\mathbf{I}_\beta$), on other viewpoint, can also be classified into the following four parts, i.e., balanced active component [$\mathrm{P_B}$; i.e., $\mathbf{I}_{\alpha\mathrm{bp}}$ (or $\mathbf{I}_{\beta\mathrm{bp}}$)], unbalanced active component [$\mathrm{P_{UB}}$; i.e., $\mathbf{I}_{\alpha\mathrm{ubp}}$ (or $\mathbf{I}_{\beta\mathrm{ubp}}$)], balanced reactive component [$\mathrm{Q_B}$; i.e., $\mathbf{I}_{\alpha\mathrm{bq}}$ (or $\mathbf{I}_{\beta\mathrm{bq}}$)], and unbalanced reactive component [$\mathrm{Q_{UB}}$; i.e., $\mathbf{I}_{\alpha\mathrm{ubq}}$ (or $\mathbf{I}_{\beta\mathrm{ubq}}$)]. The phasor diagram of the primary three-phase currents in the action of the

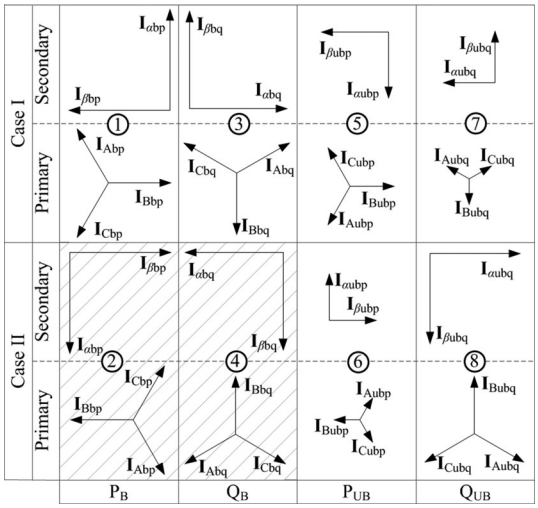

Fig. 4. Phasor relationships of all cases between primary and secondary currents.

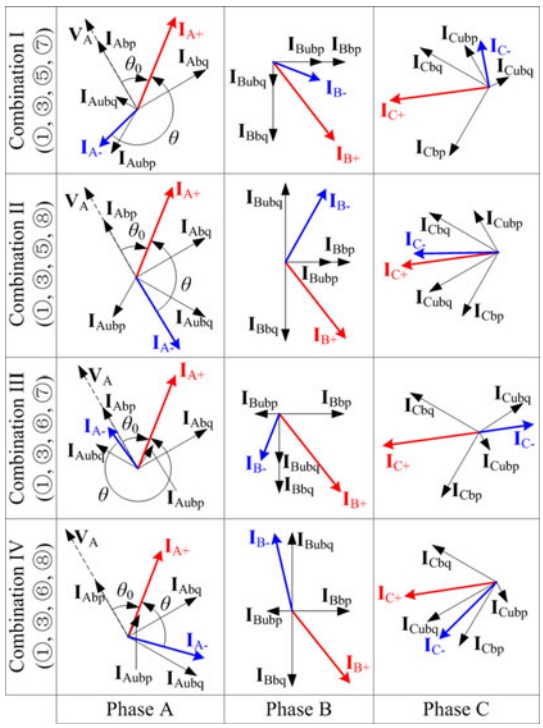

Fig. 5. Phasor relationships of the primary currents from the viewpoint of four components.

above four parts of load currents is shown in Fig. 4 accordingly. Theoretically, there are two cases (Case I and Case II) for each component, depending on the signs and amplitudes of the active power and reactive power of phase-α and -β systems, making a total of eight cases (labeled with numbers, i.e. ①to ⑧in Fig. 4). Besides, one point should be noticed in Fig. 4 is that, ②and ④in Case II correspond to the regeneration condition for $\mathrm{P_B}$ and leading condition for $\mathrm{Q_B}$, which seldom appears in ERPS occupied by ac–dc trains, so it is not included in our following analysis.

It can be observed from Fig. 4 that the primary PSC (clockwise: A→B→C) and NSC (clockwise: A→C→B) are composed of $\mathrm{P_B}$, $\mathrm{Q_B}$ and $\mathrm{P_{UB}}$, $\mathrm{Q_{UB}}$, respectively. Considering the actual load currents so do the actual primary currents, based on the superposition principle, are the combination of the cases shown in Fig. 4. Clearly, four Combinations, i.e. (①, ③, ⑤, ⑦), (①, ③, ⑤, ⑧), (①, ③, ⑥, ⑦), (①, ③, ⑥, ⑧), can be constructed. To fully discover the distribution states of NSC and PSC in the primary side, the Combinations of the primary currents are plotted in Fig. 5 under the frame defined by (5). It can be seen in Fig. 5, $\mathbf{I}_{\mathrm{kbp}}$ and $\mathbf{I}_{\mathrm{kbq}}$, which synthetize $\mathbf{I}_{\mathrm{k+}}$, are transformed from $\mathrm{P_B}$ and $\mathrm{Q_B}$, respectively; while $\mathbf{I}_{\mathrm{kubp}}$ and $\mathbf{I}_{\mathrm{kubq}}$, as the components of $\mathbf{I}_{\mathrm{k-}}$, are transformed from $\mathrm{P_{UB}}$ and $\mathrm{Q_{UB}}$, respectively (k = A, B, and C). That is to say, all balanced (or unbalanced) parts of the load currents will generate PSC (or NSC) in the primary side. Therefore, referring to Figs. 4 and 5 and the derivation process of (9), $\mathrm{I_{unb}}$ can be calculated as

$$\mathrm{I_{unb}} = \frac{I_-}{I_+} = \frac{\sqrt{{I_{\mathrm{Aubp}}}^2 + {I_{\mathrm{Aubq}}}^2}}{\sqrt{{I_{\mathrm{Abp}}}^2 + {I_{\mathrm{Abq}}}^2}} = \frac{\sigma\sqrt{{I_{\alpha\mathrm{ubp}}}^2 + {I_{\alpha\mathrm{ubq}}}^2}}{\sigma\sqrt{{I_{\alpha\mathrm{bp}}}^2 + {I_{\alpha\mathrm{bq}}}^2}} = \frac{\sqrt{{I_{\alpha\mathrm{ubp}}}^2 + {I_{\alpha\mathrm{ubq}}}^2}}{\sqrt{{I_{\alpha\mathrm{bp}}}^2 + {I_{\alpha\mathrm{bq}}}^2}}. \quad (13)$$

From (9), we can deduce the primary currents inducted by any perpendicular currents of the secondary two-phase system are σ times to the corresponding secondary parts. If we decompose the primary currents into active and reactive parts, i.e., I_{Ap}, I_{Bp}, I_{Cp} and I_{Aq}, I_{Bq}, I_{Cq}, based on $\mathbf{V}_{\mathrm{A}}$, $\mathbf{V}_{\mathrm{B}}$, and $\mathbf{V}_{\mathrm{C}}$ (note: current lags voltage means reactive part > 0), referring to Fig. 4, the coefficients of those components in cases ① to ⑧ can be calculated and listed in Table I.

According to the coefficients in Table I, take Combination I (①, ③, ⑤, ⑦) as an example, we have

$$\begin{cases} I_{\mathrm{Ap}} = \overbrace{\sigma I_{\alpha\mathrm{bp}}}^{①} + \overbrace{0I_{\alpha\mathrm{bq}}}^{③} + \overbrace{(-1/2\sigma I_{\alpha\mathrm{ubp}})}^{⑤} + \overbrace{\sqrt{3}/2\sigma I_{\alpha\mathrm{ubq}}}^{⑦} \\ I_{\mathrm{Bp}} = \sigma I_{\alpha\mathrm{bp}} + 0I_{\alpha\mathrm{bq}} + \sigma I_{\alpha\mathrm{ubp}} + 0I_{\alpha\mathrm{ubq}} \\ I_{\mathrm{Cp}} = \sigma I_{\alpha\mathrm{bp}} + 0I_{\alpha\mathrm{bq}} + (-1/2\sigma I_{\alpha\mathrm{ubp}}) + (-\sqrt{3}/2\sigma I_{\alpha\mathrm{ubq}}) \end{cases} \quad (14)$$

and

$$\begin{cases} I_{\mathrm{Aq}} = \overbrace{0I_{\alpha\mathrm{bp}}}^{①} + \overbrace{\sigma I_{\alpha\mathrm{bq}}}^{③} + \overbrace{(-\sqrt{3}/2\sigma I_{\alpha\mathrm{ubp}})}^{⑤} + \overbrace{(-1/2\sigma I_{\alpha\mathrm{ubq}})}^{⑦} \\ I_{\mathrm{Bq}} = 0I_{\alpha\mathrm{bp}} + \sigma I_{\alpha\mathrm{bq}} + 0I_{\alpha\mathrm{ubp}} + \sigma I_{\alpha\mathrm{ubq}} \\ I_{\mathrm{Cq}} = 0I_{\alpha\mathrm{bp}} + \sigma I_{\alpha\mathrm{bq}} + \sqrt{3}/2\sigma I_{\alpha\mathrm{ubp}} + (-1/2\sigma I_{\alpha\mathrm{ubq}}). \end{cases} \quad (15)$$

Inserting (14) and (15) into (11), $\mathrm{PF_f}$ can be calculated as

$$\mathrm{PF_f} = \frac{\sum_{\mathrm{k=A,B,C}} I_{\mathrm{kp}}}{\sum_{\mathrm{k=A,B,C}} \sqrt{({I_{\mathrm{kp}}}^2 + {I_{\mathrm{kq}}}^2)}} = \frac{3\sigma I_{\alpha\mathrm{bp}}}{\sigma\left(\sqrt{\left(\frac{(3I_{\alpha\mathrm{p}} + I_{\beta\mathrm{p}})}{4} + \frac{\sqrt{3}(I_{\beta\mathrm{q}} - I_{\alpha\mathrm{q}})}{4}\right)^2 + \left(\frac{\sqrt{3}(I_{\alpha\mathrm{p}} - I_{\beta\mathrm{p}})}{4} + \frac{(3I_{\alpha\mathrm{q}} + I_{\beta\mathrm{q}})}{4}\right)^2}\right.}$$

TABLE I
COEFFICIENTS BETWEEN THE AMPLITUDE OF LOAD CURRENTS AND THAT OF ACTIVE AND REACTIVE COMPONENTS OF PRIMARY CURRENTS

Cases	Primary side currents					
	Active power component			Reactive power component		
	Phase A	Phase B	Phase C	Phase A	Phase B	Phase C
①	σ	σ	σ	0	0	0
②	$-\sigma$	$-\sigma$	$-\sigma$	0	0	0
③	0	0	0	σ	σ	σ
④	0	0	0	$-\sigma$	$-\sigma$	$-\sigma$
⑤	$-1/2\sigma$	σ	$-1/2\sigma$	$-\sqrt{3}/2\sigma$	0	$\sqrt{3}/2\sigma$
⑥	$1/2\sigma$	$-\sigma$	$1/2\sigma$	$\sqrt{3}/2\sigma$	0	$-\sqrt{3}/2\sigma$
⑦	$\sqrt{3}/2\sigma$	0	$-\sqrt{3}/2\sigma$	$-1/2\sigma$	σ	$-1/2\sigma$
⑧	$-\sqrt{3}/2\sigma$	0	$\sqrt{3}/2\sigma$	$1/2\sigma$	$-\sigma$	$1/2\sigma$

$$+\sqrt{{I_{\beta \mathrm{p}}}^2+{I_{\beta \mathrm{q}}}^2} +\sqrt{\left(\frac{(3I_{\alpha \mathrm{p}}+I_{\beta \mathrm{p}})}{4}+\frac{\sqrt{3}(I_{\alpha \mathrm{q}}-I_{\beta \mathrm{q}})}{4}\right)^2 +\left(\frac{\sqrt{3}(I_{\beta \mathrm{p}}-I_{\alpha \mathrm{p}})}{4}+\frac{(3I_{\alpha \mathrm{q}}+I_{\beta \mathrm{q}})}{4}\right)^2} \tag{16}$$

It can be verified that, though (16) is derived according to Combination I (①, ③, ⑤, ⑦), it is also correct for other three combinations shown in Fig. 5.

On the other hand, the amplitude sum of the primary currents is

$$\sum_{k=\mathrm{A,B,C}} I_k = |\mathbf{I}_{\mathrm{A}+}+\mathbf{I}_{\mathrm{A}-}|+|\mathbf{I}_{\mathrm{B}+}+\mathbf{I}_{\mathrm{B}-}|+|\mathbf{I}_{\mathrm{C}+}+\mathbf{I}_{\mathrm{C}-}|\,. \tag{17}$$

If we take $\mathbf{V}_{\mathrm{A}}$ as a reference, referring to Fig. 5, the primary PSC and NSC in phase A, B, and C can be expressed as

$$\begin{cases} \mathbf{I}_{\mathrm{A}+} = \sqrt{{I_{\mathrm{Abp}}}^2+{I_{\mathrm{Abq}}}^2}\angle\theta_0 \\ \quad = \sigma\sqrt{{I_{\alpha\mathrm{bp}}}^2+{I_{\alpha\mathrm{bq}}}^2}\angle\theta_0 \\ \mathbf{I}_{\mathrm{A}-} = \sqrt{{I_{\mathrm{Aubp}}}^2+{I_{\mathrm{Aubq}}}^2}\angle(\theta_0-\theta) \\ \quad = \sigma\sqrt{{I_{\alpha\mathrm{ubp}}}^2+{I_{\alpha\mathrm{ubq}}}^2}\angle(\theta_0-\theta) \\ \mathbf{I}_{\mathrm{B}+} = \sqrt{{I_{\mathrm{Bbp}}}^2+{I_{\mathrm{Bbq}}}^2}\angle(\theta_0-120^\circ) \\ \quad = \sigma\sqrt{{I_{\alpha\mathrm{bp}}}^2+{I_{\alpha\mathrm{bq}}}^2}\angle(\theta_0-120^\circ) \\ \mathbf{I}_{\mathrm{B}-} = \sqrt{{I_{\mathrm{Bubp}}}^2+{I_{\mathrm{Bubq}}}^2}\angle(\theta_0+120^\circ-\theta) \\ \quad = \sigma\sqrt{{I_{\alpha\mathrm{ubp}}}^2+{I_{\alpha\mathrm{ubq}}}^2}\angle(\theta_0+120^\circ-\theta) \\ \mathbf{I}_{\mathrm{C}+} = \sqrt{{I_{\mathrm{Cbp}}}^2+{I_{\mathrm{Cbq}}}^2}\angle(\theta_0+120^\circ) \\ \quad = \sigma\sqrt{{I_{\alpha\mathrm{bp}}}^2+{I_{\alpha\mathrm{bq}}}^2}\angle(\theta_0+120^\circ) \\ \mathbf{I}_{\mathrm{C}-} = \sqrt{{I_{\mathrm{Cubp}}}^2+{I_{\mathrm{Cubq}}}^2}\angle(\theta_0-120^\circ-\theta) \\ \quad = \sigma\sqrt{{I_{\alpha\mathrm{ubp}}}^2+{I_{\alpha\mathrm{ubq}}}^2}\angle(\theta_0-120^\circ-\theta) \end{cases} \tag{18}$$

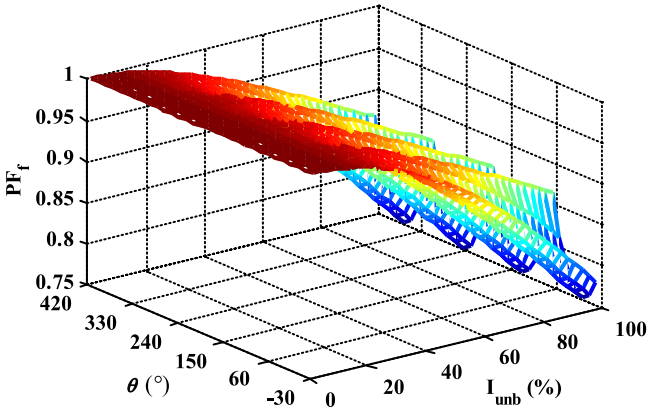

Fig. 6. Relationships of $\mathrm{PF_f}$ versus $\mathrm{I_{unb}}$ and θ.

where θ_0 is the impedance angle of PSC in phase A, and the phase difference between PSC and NSC in phase A, i.e., θ,

$$\text{satisfies} \begin{cases} 150^\circ \le \theta \le 330^\circ, & \text{Combination I} \\ 60^\circ \le \theta \le 240^\circ, & \text{Combination II} \\ 240^\circ \le \theta \le 420^\circ, & \text{Combination III} \\ -30^\circ \le \theta \le 150^\circ, & \text{Combination IV} \end{cases}.$$

Inserting (18) into (17), and $\sum_{\mathrm{k=A,B,C}} I_{\mathrm{k}}$ can be calculated as

$$\begin{aligned} \sum_{\mathrm{k=A,B,C}} I_{\mathrm{k}} = \sigma\sqrt{{I_{\alpha\mathrm{bp}}}^2+{I_{\alpha\mathrm{bq}}}^2} \\ \times(|1\angle\theta_0+I_{\mathrm{unb}}\angle(\theta_0-\theta)| \\ +|1\angle(\theta_0-120^\circ)+I_{\mathrm{unb}}\angle(\theta_0+120^\circ-\theta)| \\ +|1\angle(\theta_0+120^\circ)+I_{\mathrm{unb}}\angle(\theta_0-120^\circ-\theta)|). \end{aligned} \tag{19}$$

So combining (11), (13), (16), and (19), $\mathrm{PF_f}$ and $\mathrm{I_{unb}}$ can be finally calculated as

$$\begin{cases} \mathrm{PF_f} = \dfrac{3\mathrm{PF_{f+}}}{(|1\angle 0+I_{\mathrm{unb}}\angle(-\theta)| \\ \qquad +|1\angle(-120^\circ)+I_{\mathrm{unb}}\angle(120^\circ-\theta)| \\ \qquad +|1\angle 120^\circ+I_{\mathrm{unb}}\angle(-120^\circ-\theta)|)} \\ I_{\mathrm{unb}} = \dfrac{\sqrt{{I_{\alpha\mathrm{ubp}}}^2+{I_{\alpha\mathrm{ubq}}}^2}}{\sqrt{{I_{\alpha\mathrm{bp}}}^2+{I_{\alpha\mathrm{bq}}}^2}} \end{cases} \tag{20}$$

where $\mathrm{PF_{f+}} = \frac{I_{\mathrm{Abp}}}{\sqrt{{I_{\mathrm{Abp}}}^2+{I_{\mathrm{Abq}}}^2}} = \frac{I_{\alpha\mathrm{bp}}}{\sqrt{{I_{\alpha\mathrm{bp}}}^2+{I_{\alpha\mathrm{bq}}}^2}}$ means the fundamental power factor of the primary PSC.

From (20), we know that $\mathrm{PF_f}$ is determined by $\mathrm{PF_{f+}}$, $\mathrm{I_{unb}}$, and θ. Fig. 6 gives the relationship of $\mathrm{PF_f}$ versus $\mathrm{I_{unb}}$ and θ (here, $\mathrm{PF_{f+}} = 1$). It can be observed from Fig. 6 that $\mathrm{PF_f} \le \mathrm{PF_{f+}}$ and the bigger the $\mathrm{I_{unb}}$ is, the stronger is the influence of θ on $\mathrm{PF_f}$. Furthermore, it can be seen from Fig. 7, $\mathrm{PF_f}$ is insensitive to θ if $\mathrm{I_{unb}} \le 20\%$.

Based on the analysis stated above, three critical rules, which can be used in the following compensation strategy part, are concluded as follows:

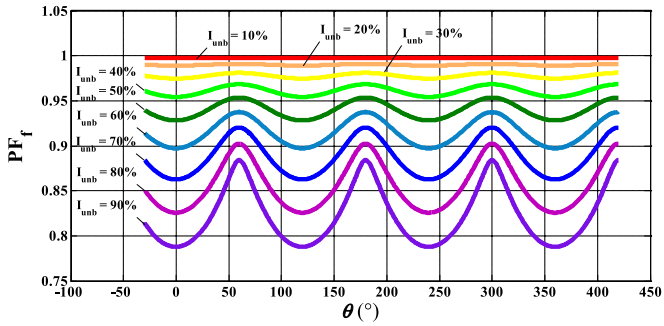

Fig. 7. Different $\mathrm{I_{unb}}$ axis sections of Fig. 6.

1) $\mathrm{PF_f}$ tends close to $\mathrm{PF_{f+}}$ ($\mathrm{PF_{f+}} \geq \mathrm{PF_f}$), if $\mathrm{I_{unb}}$ changes from a value larger than 10% to 10% (see Fig. 7).
2) The change of $\mathrm{PF_{f+}}$ has influence on $\mathrm{I_{unb}}$ because the reactive part of PSC will change when $\mathrm{PF_{f+}}$ is adjusted (see Fig. 5).
3) $\mathrm{PF_{f+}} \geq 0.9$ should be first satisfied if we want $\mathrm{PF_f} \geq 0.9$.

C. Strategy of Reactive Power Reduction and NSC Mitigation

Evaluating $\mathrm{PF_f}$ and $\mathrm{I_{unb}}$ according to (13) and (16) first, and then the following compensation strategy, which can be used to mitigate the primary reactive power and NSC, can be deduced based on the above three critical rules.

Condition 1: $\mathrm{PF_f} \geq 0.9$ and $\mathrm{I_{unb}} > 10\%$

In this condition, the main task is to reduce $\mathrm{I_{unb}}$ to a value $\leq 10\%$ by regulating $\mathrm{P_{UB}}$ and $\mathrm{Q_{UB}}$ in phase α and β (according to rule 1). Therefore, the undesired currents which should be eliminated can be calculated as

$$\begin{cases} I_{\alpha\mathrm{rp}} = {I_{\alpha\mathrm{ubp}}}^{\mathrm{ref}} = (1 - 0.1/I_{\mathrm{unb}})I_{\alpha\mathrm{ubp}} \\ I_{\alpha\mathrm{rq}} = {I_{\alpha\mathrm{ubq}}}^{\mathrm{ref}} = (1 - 0.1/I_{\mathrm{unb}})I_{\alpha\mathrm{ubq}} \\ I_{\beta\mathrm{rp}} = {I_{\beta\mathrm{ubp}}}^{\mathrm{ref}} = (1 - 0.1/I_{\mathrm{unb}})I_{\beta\mathrm{ubp}} \\ I_{\beta\mathrm{rq}} = {I_{\beta\mathrm{ubq}}}^{\mathrm{ref}} = (1 - 0.1/I_{\mathrm{unb}})I_{\beta\mathrm{ubq}} \end{cases} \tag{21}$$

where $I_{\alpha\mathrm{rp}}$, $I_{\beta\mathrm{rp}}$, $I_{\alpha\mathrm{rq}}$, and $I_{\beta\mathrm{rq}}$ are the amplitudes of the required active power and reactive power compensation currents in phase α and β, respectively. Superscript "ref" labeled currents represent the references of the corresponding currents. It is clear that $\mathrm{P_{UB}}$, and $\mathrm{Q_{UB}}$ are included in (21). For the detailed calculation process of (21), please refer to Appendix B.A.

Condition 2: $\mathrm{PF_f} \geq 0.9$ and $\mathrm{I_{unb}} \leq 10\%$

No compensation action is needed for this condition, so

$$\begin{cases} I_{\alpha\mathrm{rp}} = 0 \\ I_{\alpha\mathrm{rq}} = 0 \\ I_{\beta\mathrm{rp}} = 0 \\ I_{\beta\mathrm{rq}} = 0 \end{cases}. \tag{22}$$

Condition 3: $\mathrm{PF_f} < 0.9$ and $\mathrm{I_{unb}} > 10\%$

Step 1: Reduce $\mathrm{Q_B}$ to make $\mathrm{PF_{f+}} = 0.9$ (according to rule 3), so the currents should be compensated in this step (referring to Appendix B.B) are

$$\begin{cases} {I_{\alpha\mathrm{bq}}}^{\mathrm{ref}} = I_{\alpha\mathrm{bq}} - 0.4843 I_{\alpha\mathrm{bp}} \\ {I_{\beta\mathrm{bq}}}^{\mathrm{ref}} = I_{\beta\mathrm{bq}} - 0.4843 I_{\beta\mathrm{bp}} \end{cases}. \tag{23}$$

Step 2: Cut down a new NSC unbalance ratio $\mathrm{I_{unb}^N}$ to a value $\leq 10\%$ with the method used in Condition 1 (according to rule 1), i.e.,

$$\begin{cases} {I_{\alpha\mathrm{ubp}}}^{\mathrm{ref}} = (1 - 0.1/{\mathrm{I_{unb}}}^{\mathrm{N}})I_{\alpha\mathrm{ubp}} \\ {I_{\alpha\mathrm{ubp}}}^{\mathrm{ref}} = (1 - 0.1/{\mathrm{I_{unb}}}^{\mathrm{N}})I_{\alpha\mathrm{ubq}} \\ {I_{\beta\mathrm{ubp}}}^{\mathrm{ref}} = (1 - 0.1/{\mathrm{I_{unb}}}^{\mathrm{N}})I_{\beta\mathrm{ubp}} \\ {I_{\beta\mathrm{ubq}}}^{\mathrm{ref}} = (1 - 0.1/{\mathrm{I_{unb}}}^{\mathrm{N}})I_{\beta\mathrm{ubq}} \end{cases} \tag{24}$$

where $\mathrm{I_{unb}^N}$ is the updated NSC unbalance ratio calculated by (13) after Step 1 is implemented.

Since some balanced reactive currents are reduced by (23), the amplitude of the primary PSC will also diminish (according to rule 2). Therefore, the primary $\mathrm{I_{unb}}$ will increase to the new value $\mathrm{I_{unb}^N}$, which is not the expected value in our compensation scheme. Thus, the strategy used in Condition 1 should be adopted to suppress NSC.

Step 3: Add the two parts of the undesired currents together

$$\begin{cases} I_{\alpha\mathrm{rp}} = {I_{\alpha\mathrm{ubp}}}^{\mathrm{ref}} \\ I_{\alpha\mathrm{rq}} = {I_{\alpha\mathrm{bq}}}^{\mathrm{ref}} + {I_{\alpha\mathrm{ubq}}}^{\mathrm{ref}} \\ I_{\beta\mathrm{rp}} = {I_{\beta\mathrm{ubp}}}^{\mathrm{ref}} \\ I_{\beta\mathrm{rq}} = {I_{\beta\mathrm{bq}}}^{\mathrm{ref}} + {I_{\beta\mathrm{ubq}}}^{\mathrm{ref}} \end{cases}. \tag{25}$$

It is clear that the undesired components in (25) consist of $\mathrm{P_{UB}}$, $\mathrm{Q_{UB}}$, and $\mathrm{Q_B}$.

Condition 4: $\mathrm{PF_f} < 0.9$ and $\mathrm{I_{unb}} \leq 10\%$

Step 1: Reduce $\mathrm{Q_B}$ to make $\mathrm{PF_{f+}} = 0.9$ (according to rule 3). It is the same to that in Condition 3.

Step 2: Check whether $\mathrm{I_{unb}^N}$ still satisfies the criterion of $\mathrm{I_{unb}^N} \leq 10\%$ (according to rule 2). No more needs to be done if yes to that check, so the undesired currents are just regulated by (23). Otherwise, go to *Step 3*.

Step 3: Cut $\mathrm{I_{unb}^N}$ down to a value $\leq 10\%$ with the method used in Condition 3 (according to rule 1), so the undesired currents should be calculated by (25).

For programming convenience consideration, the flowchart for the implementation of the four conditions is given in Fig 8.

Based on the above analysis, it can be stated that if traction substations with balanced transformers (e.g., impedance match transformer or Scott transformer, so on.) will be equipped with a facility for power quality improvement, a similar compensation strategy can be introduced due to the quadrature characteristic, which is the foundation of the above analysis. As for the detailed implementation of this compensation system, it is explored in the second part of this paper.

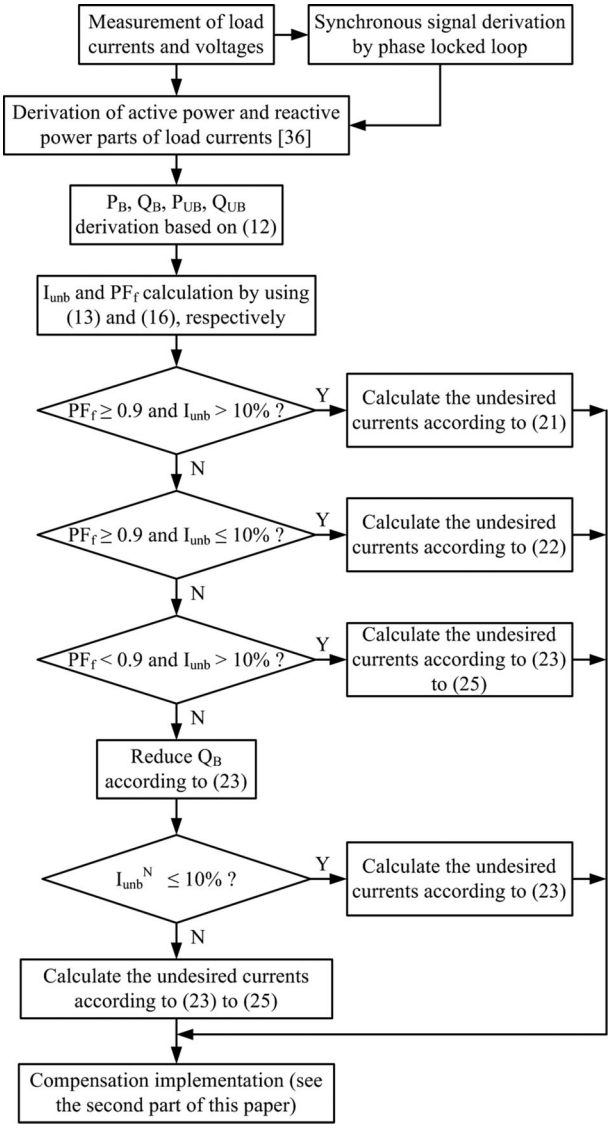

Fig. 8. Flowchart of the new partial compensation strategy.

D. Capacity Analysis

It can be seen from Fig. 3 that the two-phase load currents can be expressed as

$$\begin{cases} \mathbf{I}_\alpha = I_\alpha \angle \theta_\alpha \\ \mathbf{I}_\beta = I_\beta \angle \theta_\beta \end{cases} \tag{26}$$

where $I_\alpha, I_\beta \in [0, I_\mathrm{N}]$ and $\theta_\alpha, \theta_\beta \in [0, \theta_\mathrm{N}]$, θ_N is the maximum impedance angle of the locomotive loads.

For any two-phase loads belong to (26), two undesired currents of the proposed compensation strategy, $I_{\alpha\mathrm{r}} = (I_{\alpha\mathrm{rp}}^2 + I_{\alpha\mathrm{rq}}^2)^{0.5}$ and $I_{\beta\mathrm{r}} = (I_{\beta\mathrm{rp}}^2 + I_{\beta\mathrm{rq}}^2)^{0.5}$, can be calculated by the process shown in Fig. 8. For full compensation mode, referring to Fig. 2(b), the undesired currents can be calculated as

$$\begin{cases} I_{\alpha\mathrm{r}} = \sqrt{(I_{\alpha\mathrm{p}} - I_{\alpha\mathrm{bp}})^2 + (I_{\alpha\mathrm{q}})^2} \\ I_{\beta\mathrm{r}} = \sqrt{(I_{\beta\mathrm{p}} - I_{\beta\mathrm{bp}})^2 + (I_{\beta\mathrm{q}})^2}. \end{cases} \tag{27}$$

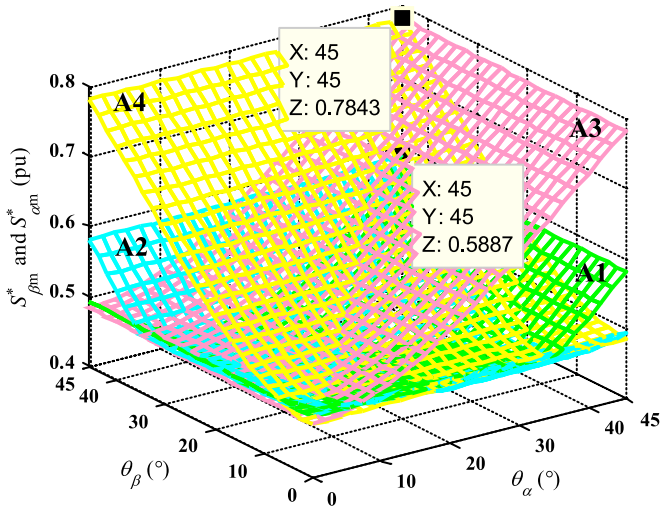

Fig. 9. Relationships of $S^*_{\alpha\mathrm{m}}$ and $S^*_{\beta\mathrm{m}}$ versus θ_α and θ_β.

Considering $I_{\alpha\mathrm{bp}} = I_{\beta\mathrm{bp}} = 0.5(I_{\beta\mathrm{p}} + I_{\alpha\mathrm{p}})$, so

$$\begin{cases} I_{\alpha\mathrm{r}} = \sqrt{\left(\frac{I_{\alpha\mathrm{p}} - I_{\beta\mathrm{p}}}{2}\right)^2 + (I_{\alpha\mathrm{q}})^2} \\ I_{\beta\mathrm{r}} = \sqrt{\left(\frac{I_{\beta\mathrm{p}} - I_{\alpha\mathrm{p}}}{2}\right)^2 + (I_{\beta\mathrm{q}})^2}. \end{cases} \tag{28}$$

Thus, the compensation VA-capacity of phase α and β, S^*_α and S^*_β [in per unit (pu) form], can be uniformly expressed as

$$\begin{cases} {S_\alpha}^* = \frac{V_\alpha I_{\alpha\mathrm{r}}}{V_\alpha I_\mathrm{N}} = f_\alpha(I_\alpha, I_\beta, \theta_\alpha, \theta_\beta) \\ {S_\beta}^* = \frac{V_\beta I_{\beta\mathrm{r}}}{V_\beta I_\mathrm{N}} = f_\beta(I_\alpha, I_\beta, \theta_\alpha, \theta_\beta) \end{cases} \tag{29}$$

where $f_\alpha(I_\alpha, I_\beta, \theta_\alpha, \theta_\beta)$ and $f_\beta(I_\alpha, I_\beta, \theta_\alpha, \theta_\beta)$ are multivariable functions.

For all $I_\alpha, I_\beta \in [0, I_\mathrm{N}]$, the relationships of the maximum values of S^*_α and S^*_β (i.e., $S^*_{\alpha\mathrm{m}}$ and $S^*_{\beta\mathrm{m}}$) versus θ_α and θ_β ($\theta_\mathrm{N} = 45°$) of the proposed partial and full compensation modes are plotted in Fig. 9 by using the M-language in MATLAB. The annotations of the four regions in Fig. 9 are as follows: region A1: phase-α converter operates with partial compensation mode; region A2: phase-β converter operates with partial compensation mode; region A3: phase-α converter operates with full compensation mode; and region A4: phase-β converter operates with full compensation mode.

It can be seen in Fig. 9 that, the VA-capacity reduction ratio of the maximum $S^*_{\alpha\mathrm{m}}$ and $S^*_{\beta\mathrm{m}}$, which occurs at the point of $\theta_\alpha = 45°$ and $\theta_\beta = 45°$, between the proposed compensation mode and full compensation mode is 25%. The reduced requirement on VA capacity, together with the simple derivation process, is the prominent advantage of the proposed partial compensation strategy.

V. Conclusion

A new system constructed with YNvd-connected balance transformer and MBTBC, along with a new power distribution strategy, is proposed in this paper for the power quality

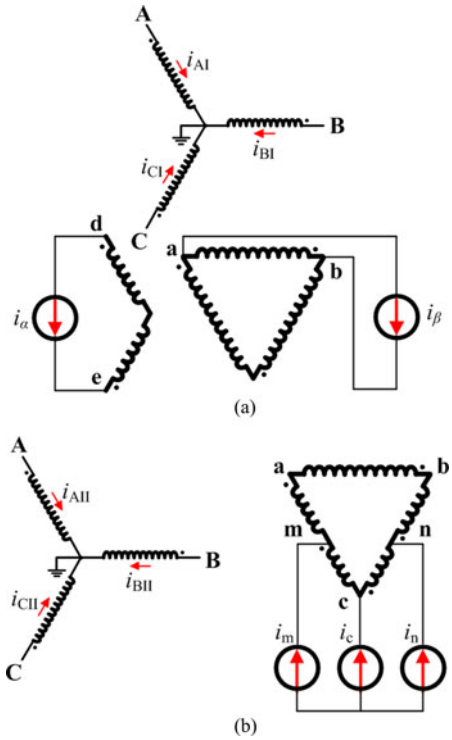

Fig. 10 Equivalent circuit of two different loading conditions. (a) Two-phase loading condition. (b) Three-phase loading condition.

improvement in ERPS. By employing MBTBC and the taps in the Δ-loop of the main transformer, only one isolation transformer is used and the system's integration level is significantly improved. Besides, according to a deep analysis of the quadrature components of the load currents and the related influence on PF_f and I_{unb} of the primary side, a new partial compensation strategy without complex calculation and optimization is explored. On the one hand, this strategy can be applied to other balance transformer installed traction substations for power quality improvement, and on the other hand, the compensation VA capacity of the converter on the proposed partial compensation mode is by 25% lower than that of the commonly used full compensation mode.

Appendix A

As stated in the beginning of Section II, YNvd-connected balance transformer can feed locomotives on phase α and β via terminal d-e and a-b [see Fig. 10(a)], respectively. Based on the regulations in (1) and the multiwinding transformer theory, the current relationship between primary and secondary sides is

$$\begin{bmatrix}\mathbf{I}_{AI}\\ \mathbf{I}_{BI}\\ \mathbf{I}_{CI}\end{bmatrix}=\frac{1}{3K}\begin{bmatrix}-\sqrt{3} & -1\\ 0 & 2\\ \sqrt{3} & -1\end{bmatrix}\begin{bmatrix}\mathbf{I}_\alpha\\ \mathbf{I}_\beta\end{bmatrix} \tag{A.1}$$

where $K = W_1/W_2 = 2.309$, and denotes the transformer ratio. It can be observed from (A.1) that the primary currents are irrelevant to x and λ, and contain no zero-sequence current.

Considering another condition, if three-phase loads are supplied through terminal m-n-c [see Fig. 10(b), note that among $\mathbf{I}_m$, $\mathbf{I}_n$, and $\mathbf{I}_c$ only two of them are independent because of the fact $\mathbf{I}_m + \mathbf{I}_n + \mathbf{I}_c = \mathbf{0}$], according to the multiwinding transformer theory and the definitions in (1), the primary currents are calculated by

$$\begin{bmatrix}\mathbf{I}_{AII}\\ \mathbf{I}_{BII}\\ \mathbf{I}_{CII}\end{bmatrix}=\frac{1}{3K}\begin{bmatrix}\lambda-3x & -\lambda\\ \lambda & -\lambda\\ \lambda & 3x-\lambda\end{bmatrix}\begin{bmatrix}\mathbf{I}_m\\ \mathbf{I}_n\end{bmatrix}. \tag{A.2}$$

To suppress zero-sequence current in the primary side, the sum of the column elements of the coefficient matrix in (A.2) should equal to zero, i.e., $3x - 3\lambda = 0$, which leads to $x = \lambda$.

Appendix B

A. Controlling Method of I_{unb}

From the second equation of (20), we have

$$\sqrt{{I_{\alpha ubp}}^2+{I_{\alpha ubq}}^2}=I_{unb}\sqrt{{I_{\alpha bp}}^2+{I_{\alpha bq}}^2}. \tag{B.1}$$

It is supposed that I_{unb} in (B.1) is larger than 0.1 (i.e. 10%). On the other hand, inserting a pair of satisfactory unbalanced active and reactive currents ${I_{\alpha ubp}}^s$ and ${I_{\alpha ubq}}^s$, which makes $I_{unb} = 0.1$, into the second equation of (20), i.e.,

$$\sqrt{({I_{\alpha ubp}}^s)^2+({I_{\alpha ubq}}^s)^2}=0.1\sqrt{{I_{\alpha bp}}^2+{I_{\alpha bq}}^2}. \tag{B.2}$$

Here, we suppose P_B and Q_B in phase α are constant. Subtracting (B.2) from (B.1) will lead to

$$\begin{aligned}&\sqrt{{I_{\alpha ubp}}^2+{I_{\alpha ubq}}^2}-\sqrt{({I_{\alpha ubp}}^s)^2+({I_{\alpha ubq}}^s)^2}\\ &=(I_{unb}-0.1)\sqrt{{I_{\alpha bp}}^2+{I_{\alpha bq}}^2}.\end{aligned} \tag{B.3}$$

Dividing (B.3) by (B.1) and making a simplification, it can be obtained that

$$\begin{aligned}\sqrt{({I_{\alpha ubp}}^s)^2+({I_{\alpha ubq}}^s)^2}=&\left(1-\underbrace{\frac{I_{unb}-0.1}{I_{unb}}}_{k}\right)\\ &\sqrt{{I_{\alpha ubp}}^2+{I_{\alpha ubq}}^2}.\end{aligned} \tag{B.4}$$

To satisfy (B.4), a simple implementation method is to proportionally adjust the corresponding currents with ratio $1 - k$, this is to say,

$$\begin{cases}{I_{\alpha ubp}}^s=(1-k){I_{\alpha ubp}}\\ {I_{\alpha ubq}}^s=(1-k){I_{\alpha ubq}}.\end{cases} \tag{B.5}$$

From (B.5), the undesired currents ${I_{\alpha bp}}^{ref}$ and ${I_{\alpha bq}}^{ref}$, which should be eliminated in phase α to regulate I_{unb}, can be calculated as

$$\begin{cases}{I_{\alpha ubp}}^{ref}={I_{\alpha ubp}}-{I_{\alpha ubp}}^s=(1-0.1/I_{unb}){I_{\alpha ubp}}\\ {I_{\alpha ubq}}^{ref}={I_{\alpha ubq}}-{I_{\alpha ubq}}^s=(1-0.1/I_{unb}){I_{\alpha ubq}}.\end{cases} \tag{B.6}$$

Similarly, the counterpart in phase β can be derived as

$$\begin{cases}{I_{\beta ubp}}^{ref}=(1-0.1/I_{unb}){I_{\beta ubp}}\\ {I_{\beta ubq}}^{ref}=(1-0.1/I_{unb}){I_{\beta ubq}}.\end{cases} \tag{B.7}$$

B. Controlling Method of $\mathrm{PF_{f+}}$

Assuming $\mathrm{PF_{f+}}$ in (20) equals to 0.9, i.e.,

$$\mathrm{PF_{f+}} = I_{\alpha\mathrm{bp}} \Big/ \sqrt{{I_{\alpha\mathrm{bp}}}^2 + {I_{\alpha\mathrm{bq}}}^2} = 0.9. \tag{B.8}$$

From (B.8), ${I_{\alpha\mathrm{bq}}}^{\mathrm{s}}$ the satisfactory balanced reactive power current in phase α in the condition of $\mathrm{PF_{f+}} = 0.9$, can be obtained as

$${I_{\alpha\mathrm{bq}}}^{\mathrm{s}} = 0.4843 I_{\alpha\mathrm{bp}}. \tag{B.9}$$

If $I_{\alpha\mathrm{bp}}$ is larger than ${I_{\alpha\mathrm{bq}}}^{\mathrm{s}}$, which can lead to $\mathrm{PF_{f+}} < 0.9$, the required reactive compensation current in phase α, i.e., $I_{\alpha\mathrm{bq}}^{\mathrm{ref}}$, can be calculated as

$${I_{\alpha\mathrm{bq}}}^{\mathrm{ref}} = I_{\alpha\mathrm{bq}} - {I_{\alpha\mathrm{bq}}}^{\mathrm{s}} = I_{\alpha\mathrm{bq}} - 0.4843 I_{\alpha\mathrm{bp}}. \tag{B.10}$$

Similarly, the counterpart in phase β can be derived as

$${I_{\beta\mathrm{bq}}}^{\mathrm{ref}} = I_{\beta\mathrm{bq}} - 0.4843 I_{\beta\mathrm{bp}}. \tag{B.11}$$

REFERENCES

[1] S. M. M. Gazafrudi, A. T. Langerudy, E. F. Fuchs, and K. AI-Haddad, "Power quality issues in railway electrification: A comprehensive perspective," *IEEE Trans. Ind. Electron.*, vol. 62, no. 5, pp. 3081–3090, May 2015.

[2] A. Župan, A. T. Teklić, and B. F. Grčić, "Modeling of 25kV electric railway system for power quality studies," in *Proc. EUROCON Conf.*, 2013, pp. 844–849.

[3] Z. He, H. Hu, Y. Zhang, and S. Gao, "Harmonic resonance assessment to traction power-supply system considering train model in China high-speed railway," *IEEE Trans. Power Del.*, vol. 29, no. 7, pp. 1735–1743, Aug. 2014.

[4] H. Hu, Z. He, X. Li, K. Wang, and S. Gao, "Power quality impact assessment for high-speed railway associated with high-speed trains using train timetable—Part I: Methodology and modeling," *IEEE Trans. Power Del.*, vol. 31, no. 2, pp. 693–703, Apr. 2016.

[5] S. R. Sama, S. Paul, and S. H. N. Dey, "Elimination of partial overloading of generators under unbalanced operating conditions of power systems," *CSEE J. Power Energy Syst.*, vol. 2, no. 1, pp. 81–87, Mar. 2016.

[6] D. Zhang, Z. Zhang, W. Wang, and Y. Yang, "Negative sequence current optimizing control based on railway static power conditioner in V/v traction power supply system," *IEEE Trans. Power Electron.*, vol. 31, no. 1, pp. 200–212, Jan. 2016.

[7] S. Bhattacharya, P. T. Cheng, and D. M. Divan, "Hybrid solutions for improving passive filter performance in high power applications," *IEEE Trans. Ind. Appl.*, vol. 33, no. 3, pp. 732–747, May/Jun. 1997.

[8] J. C. Das, "Passive filters—Potentialities and limitations," *IEEE Trans. Ind. Appl.*, vol. 4, no. 1, pp. 232–241, Jan./Feb. 2004.

[9] D. Rivas, L. Morán, J. W. Dixon, and J. R. Espinoza, "Improving passive filter compensation performance with active techniques," *IEEE Trans. Ind. Electron.*, vol. 50, no. 1, pp. 161–170, Feb. 2003.

[10] S. Senini and P. J. Wolfs, "Hybrid active filter for harmonically unbalanced three phase three wire railway traction loads," *IEEE Trans. Power Electron.*, vol. 15, no. 4, pp. 702–710, Jul. 2000.

[11] Z. Zhang, B. Wu, J. Kang, and L. Luo, "A multi-purpose balanced transformer for railway traction applications," *IEEE Trans. Power Del.*, vol. 24, no. 2, pp. 711–718, Apr. 2009.

[12] L. Battistelli, D. Lauria, and D. Proto, "Two-phase controlled compensator for alternating-current quality improvement of electrified railway systems," *IEE Proc. Electron. Power Appl.*, vol. 153, no. 2, pp. 177–183, Mar. 2006.

[13] H. Wang, Y. Liu, K. Yan, Y. Fu, and C. Zhang, "Analysis of static var compensators installed in different positions in electric railways," *IET Elect. Syst. Transp.*, vol. 5, no. 3, pp. 129–134, 2015.

[14] G. Zhu, J. Chen, and X. Liu, "Compensation for the negative-sequence currents of electric railway based on SVC," in *Proc. 3rd IEEE Conf. Ind. Electron. Appl.*, 2008, pp. 1958–1963.

[15] T. Uzuka, "Faster than a speeding bullet: An overview of Japanese high-speed rail technology and electrification," *IEEE Electrific. Mag.*, vol. 1, no. 1, pp. 11–20, Sep. 2013.

[16] C. Wang, X. Yin, Z. Zhang, and M. Wen, "A novel compensation technology of static synchronous compensator integrated with distribution transformer," *IEEE Trans. Power Del.*, vol. 28, no. 2, pp. 1032–1039, Apr. 2013.

[17] M. Molinas, J. A. Suul, and T. Undeland, "Low voltage ride through of wind farms with cage generators: STATCOM versus SVC," *IEEE Trans. Power Electron.*, vol. 23, no. 3, pp. 1104–1117, May 2008.

[18] S. Babaei, B. Fardanesh, and S. Bhattacharya, "High-power VSC-based simultaneous positive- and negative-sequence voltage regulator," *IEEE Trans. Power Del.*, vol. 29, no. 5, pp. 2124–2135, Oct. 2014.

[19] T. L. Lee, S. H. Hu, and Y. H. Chan, "D-STATCOM with positive-sequence admittance and negative-sequence conductance to mitigate voltage fluctuations in high-level penetration of distributed-generation systems," *IEEE Trans. Ind. Electron.*, vol. 60, no. 4, pp. 1417–1428, Apr. 2013.

[20] Q. Song and W. Liu, "Control of a cascaded STATCOM with star configuration under unbalanced conditions," *IEEE Trans. Power Electron.*, vol. 24, no. 1, pp. 45–58, Jan. 2009.

[21] D. Soto and T. C. Green, "A comparison of high-power converter topologies for the implementation of FACTS controllers," *IEEE Trans. Ind. Electron.*, vol. 49, no. 5, pp. 1072–1080, Oct. 2002.

[22] A. Bueno, J. M. Aller, J. A. Restrepo, R. Harley, and T. G. Habetler, "Harmonic and unbalance compensation based on direct power control for electric railway systems," *IEEE Trans. Power Electron.*, vol. 28, no. 12, pp. 5823–5831, Dec. 2013.

[23] P. Tan, P. C. Loh, and D. G. Holmes, "A robust multilevel hybrid compensation system for 25-kV electrified railway applications," *IEEE Trans. Power Electron.*, vol. 19, no. 4, pp. 1043–1052, Jul. 2004.

[24] K. M. Kwon, Y. S. Song, and J. Choi, "6MVA single-phase APF for high speed train line in Korea," in *Proc. Int. Conf. Power Eng. Renewable Energy*, 2014, pp. 31–36.

[25] Z. Sun, X. Jiang, D. Zhu, and G. Zhang, "A novel active power quality compensator topology for electrified railway," *IEEE Trans. Power Electron.*, vol. 19, no. 4, pp. 1036–1042, Jul. 2004.

[26] Y. Horita, N. Morishima, M. Kai, M. Onishi, T. Masui, and M. Noguchi, "Single-phase STATCOM for feeding system of Tokaido Shinkansen," in *Proc. Int. Power Electron. Conf.*, 2010, pp. 2165–2170.

[27] S. Hu *et al.*, "A power factor-oriented railway power flow controller for power quality improvement in electrical railway power system," *IEEE Trans. Ind. Electron.*, vol. 64, no. 2, pp. 1167–1177, Feb. 2017.

[28] S. Hu *et al.*, "A new integrated hybrid power quality control system for electrical railway," *IEEE Trans. Ind. Electron.*, vol. 62, no. 10, pp. 6222–6232, Oct. 2015.

[29] Y. Li *et al.*, "A virtual impedance comprehensive control strategy for the controllably inductive power filtering system," *IEEE Trans. Power Electron.*, vol. 32, no. 2, pp. 920–926, Feb. 2017.

[30] B. Chen, C. Zhang, C. Tian, J. Wang, and J. Yuan, "A hybrid electrical magnetic power quality compensation system with minimum active compensation capacity for V/V cophase railway power supply system," *IEEE Trans. Power Electron.*, vol. 31, no. 6, pp. 4159–4170, Jun. 2016.

[31] Y. Li, T. K. Saha, O. Krause, Y. Cao, and C. Rehtanz, "An inductively active filtering method for power-quality improvement of distribution networks with nonlinear loads," *IEEE Trans. Power Del.*, vol. 28, no. 4, pp. 2465–2473, Oct. 2013.

[32] N. Y. Dai, M. C. Wong, K. W. Lao, and C. K. Wong, "Modelling and control of a railway power conditioner in co-phase traction power system under partial compensation," *IET Power Electron*., vol. 7, no. 5, pp. 1044–1054, 2013.

[33] N. Y. Dai, K. W. Lao, and C. S. Lam, "Hybrid railway power conditioner with partial compensation for converter rating reduction," *IEEE Trans. Ind. Appl.*, vol. 51, no. 5, pp. 4130–4138, Sep./Oct. 2015.

[34] S. Jiang, Y. Zhou, G. Liu, and X. Luo, "Operation characteristic analysis and model tests of Y/>/Δ connected balance transformer," *Proc. CESS, Soc*., vol. 23, no. 4, pp. 102–106, Apr. 2003.

[35] Quality of Electric Energy Supply Admissible Three Phase Voltage Unbalance, National Standard GB/T 15543-2008.

[36] H. Akagi, E. H. Watanabe, and M. Aredes, *Instantaneous Power Theory and Applications to Power Conditioning*. Hoboken, NJ, USA: Wiley, 2007.

Zhiwen Zhang received the B.Sc. and M.Sc. degrees in electrical engineering and Ph.D. degree in control theory and control engineering from Hunan University, Changsha, China, in 1987, 1990, and 2006, respectively.

From 1992 to 1993, he was a visiting scholar at Tsinghua University, Beijing, China, and from 2006 to 2007, he was a Visiting Professor at Ryerson University, Toronto, ON, Canada, respectively. He is currently a Full Professor in the College of Electrical and Information Engineering, Hunan University. His research interests include theory and new technology of ac/dc energy transform, theory and application of new-type electric apparatus, harmonic suppression for electric railway, power electronics application, and computer control.

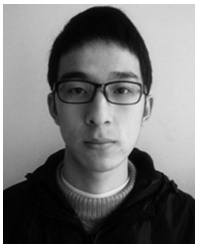

Bin Xie was born in Hunan, China, in 1990. He received the B.Sc. degree in electrical engineering from Shaoyang University, Shaoyang, China, in 2013. He is currently working toward the Ph.D. degree of electrical engineering in the College of Electrical and Information Engineering, Hunan University, Changsha, China.

His research interests include power quality analysis and compensation strategy of electrical railway power systems, renewable energy, and high-power applications of converters.

Sijia Hu (S'14–M'16) was born in Hunan, China, in 1987. He received the B.Sc. and Ph.D. degrees in electrical engineering (and automation) from Hunan University of Science and Technology, Xiangtan, China, and Hunan University (HNU), Changsha, China, in 2010 and 2015, respectively.

Since May 2016 and February 2017, he has been an Assistant Professor of electrical engineering at HNU, and a Research Fellow in Power and Energy System in the School of Information Technology and Electrical Engineering, University of Queensland, Brisbane, QLD, Australia, respectively. His research interests include: power quality, power flow control, and system modeling of high-speed railway power system; state estimation under measurement deficiency and power system load ability determination of distribution power system; new topology converters and power flow controller design and optimization; and stability analyses and control of multiconverter interactive systems.

Yong Li (S'09–M'12–SM'14) was born in Henan, China, in 1982. He received the B.Sc. and Ph.D. degrees from the College of Electrical and Information Engineering, Hunan University, Changsha, China, in 2004 and 2011, respectively, and the second Ph.D. degree from Institute of Energy Systems, Energy Efficiency, and Energy Economics (ie3), TU Dortmund University, Dortmund, Germany, in 2012.

Since 2009, he worked as a Research Associate at ie3. After then, he was a Research Fellow with the University of Queensland, Brisbane, QLD, Australia. Since 2014, he is a Full Professor of electrical engineering at Hunan University. His current research interests include power system stability analysis and control, ac/dc energy conversion systems and equipment, analysis and control of power quality, and HVdc and FACTS technologies.

Dr. Li is a member of the Association for Electrical, Electronic and Information Technologies (VDE) in Germany.

Longfu Luo (M'09) was born in Hunan, China, in 1962. He received the B.Sc., M.Sc., and Ph.D. degrees from the College of Electrical and Information Engineering, Hunan University, Changsha, China, in 1983, 1991, and 2001, respectively.

From 2001 to 2002, he was a Senior Visiting Scholar at the University of Regina, Regina, SK, Canada. He is currently a Full Professor of electrical engineering in the College of Electrical and Information Engineering, Hunan University. His research interests include the design and optimization of modern electrical equipment, the development of new converter transformer, and the study of corresponding new HVdc theories.

Christian Rehtanz (M'96–SM'06) was born in Germany in 1968. He received the Diploma and Ph.D. degrees in electrical engineering from TU Dortmund University, Dortmund, Germany, in 1994 and 1997, respectively. He received the *venia legend* in electrical power systems from the Swiss Federal Institute of Technology, Zurich, Switzerland, in 2003.

In 2000, he joined ABB Corporate Research, Baden, Switzerland. He became the Head of Technology for the global ABB business area of power systems in 2003, and the Director of ABB Corporate Research, Beijing, China, in 2005. Since 2007, he has been the Head of the Institute of Energy Systems, Energy Efficiency and Energy Economics (ie3), TU Dortmund University. In addition, he has been a Scientific Advisor of ef.Ruhr GmbH, Dortmund, a joint research company of the three universities of Bochum, Dortmund, and Duisburg-Essen (University Alliance Metropolis Ruhr) since 2007. He is an Adjunct Professor with Hunan University, Changsha, China. He has authored more than 150 scientific publications, 3 books, and 17 patents and patent applications. His research interests include electrical power systems and power economics, technologies for network enhancement and congestion relief, such as stability assessment, wide-area monitoring, protection, coordinated network-control, and integration and control of distributed generation and storage.

Dr. Rehtanz received the MIT World Top 100 Young Innovators Award 2003.

Olav Krause (M'05) was born in Germany in 1978. He received the Dipl.-Ing. (M.E.) and Dr.-Ing. (Ph.D.) degrees in electrical engineering from the TU Dortmund University, Dortmund, Germany, in 2005 and 2009, respectively.

He is currently a Lecturer of electrical engineering in the School of Information Technology and Electrical Engineering, the University of Queensland, Brisbane, QLD, Australia. His main research interests include distribution network automation, with a focus on state estimation under measurement deficiency and power system load ability determination. This is complemented by work on techniques of probabilistic and harmonic power-flow analysis.